JAMES | Journal of Advances in Modeling Earth Systems

RESEARCH ARTICLE
10.1029/2023MS003699

# The Impact of Radiative Transfer at Reduced Spectral Resolution in Large-Eddy Simulations of Convective Clouds

**M. A. Veerman[1], R. Pincus[2], E. J. Mlawer[3], and C. C. van Heerwaarden[1]**

[1]Meteorology and Air Quality Group, Wageningen University & Research, Wageningen, The Netherlands, [2]Lamont-Doherty Earth Observatory, Columbia University, New York, Palisades, NY, USA, [3]Atmospheric and Environmental Research, Lexington, MA, USA

**Key Points:**

- We investigate the sensitivity of moist convection to the spectral detail of gas optics
- We perform multiple large-eddy simulations, with progressively smaller *k*-distributions, for three case studies of convective clouds
- Mean differences in simulated cloud properties are relatively small compared to temporal fluctuations

**Correspondence to:**

M. A. Veerman,
menno.veerman@wur.nl

**Citation:**

Veerman, M. A., Pincus, R., Mlawer, E. J., & van Heerwaarden, C. C. (2024). The impact of radiative transfer at reduced spectral resolution in large-eddy simulations of convective clouds. *Journal of Advances in Modeling Earth Systems*, *16*, e2023MS003699. https://doi.org/10.1029/2023MS003699

Received 1 MAR 2023
Accepted 23 NOV 2023



**Abstract** Many radiative transfer schemes approximate the spectral integration over $\sim 10^5$ to $\sim 10^6$ wavelengths with correlated *k*-distributions methods that typically require only $10^1$–$10^2$ spectral integration points (*g*-points). The exact number of *g*-points is then chosen as an optimal balance between computational costs and accuracy, normally assessed in terms of a number of radiative quantities. How this radiative accuracy propagates to simulation accuracy, however, is not straightforward. In this study, we therefore explore the sensitivity of cloud properties in large-eddy simulations (LES) to the accuracy of radiative fluxes and heating rates. We first generate smaller sets of *g*-points from existing *k*-distributions by repeatedly combining adjacent *g*-points while maintaining the highest possible accuracy on a chosen set of radiative metrics. Next, we perform three sets of LES with varying cloud—radiation coupling pathways, and therefore different requirements for the accuracy of the radiative transfer computations, to investigate how these smaller and thus less accurate *k*-distributions affect simulation characteristics. The decrease in radiative accuracy with 3–4 times smaller *k*-distributions results in biases in cloud properties that are relative small compared to their temporal fluctuations. These results show potential for speeding up radiative transfer computations in cloud-resolving models by reducing the resolved spectral detail. However, more statistically converged simulations and a wider set of case studies is required to fully assess the robustness of our results.

**Plain Language Summary** Radiation emitted by the sun and the earth drives our weather and climate. Atmospheric models therefore need to compute how solar and thermal radiation interacts with cloud droplets, aerosols, and gas molecules. These computations can be performed very accurately by doing independent calculations for many wavelengths, but that is very time-consuming. Here, we study to what extent the accuracy of the radiation computations affects the accuracy of simulations of the atmosphere. We find that the reduction in radiative accuracy corresponding to 3–4 times fewer representative computations results in relative small mean errors in cloud properties compared to the temporal fluctuations. In further research, we should aim to better understand whether the mean errors are small enough to represent accurate simulations.

## 1. Introduction

To produce accurate simulations of clouds, atmospheric models require computationally expensive parametrizations of physical processes such as radiative transfer. The accuracy of radiative transfer computations largely depends on the spectral detail that is resolved (e.g., Hogan & Matricardi, 2022) because the absorption and scattering of radiation by the atmosphere is strongly wavelength dependent. Instead of integrating directly over all absorption lines in the solar and thermal spectra, requiring $O(10^5) - O(10^6)$ monochromatic computations, the spectral integration is often parameterized using correlated *k*-distribution or similar methods (e.g., Fu & Liou, 1992) that use just $O(10^1) - O(10^2)$ spectral quadrature points (*g*-points). Such parametrizations for spectral integration are developed to minimize errors in radiative quantities across some set of atmospheric conditions. How such errors propagate to errors in simulations of clouds and atmospheric circulation is often not clear.

The large computational costs of radiative transfer parametrizations have sparked multiple efforts to develop *k*-distributions with as few *g*-points as possible without sacrificing radiative accuracy. The widely used RRTM for General circulation model applications (RRTMG; Iacono et al., 2008), a reduced spectral resolution version of RRTM (Iacono et al., 2000; Mlawer et al., 1997), uses 140 *g*-points for longwave and 112 *g*-points for shortwave. Its successor, the more accurate Radiative Transfer for Energetics and RRTMG-Parallel (RTE + RRTMGP; Pincus et al., 2019), has a default *k*-distribution with 224 shortwave and 256 longwave *g*-points, generated using

a fixed spectral discretization, but later added more optimized *k*-distributions with just 128 longwave and 112 shortwave *g*-points. Algorithms that directly tie the spectral discretization to radiative accuracy (e.g., Hogan & Matricardi, 2022; Sekiguchi & Nakajima, 2008) typically produce more compact *k*-distributions. For example, Sekiguchi and Nakajima (2008) produced a *k*-distribution with just 40 *g*-points for shortwave and longwave radiation combined, suitable for current climate conditions. Recently, Hogan and Matricardi (2022) generated *k*-distributions with just 16 *g*-points they considered accurate enough for short-term weather forecasts and *k*-distributions with 32 *g*-points that produced accurate greenhouse gas forcings. In the aforementioned studies, *k*-distributions were optimized against highly accurate line-by-line models (Clough et al., 2005), using radiative metrics such as downwelling surface fluxes, upwelling top-of-atmosphere (TOA) fluxes, or radiative heating rates (see cost functions in Sekiguchi and Nakajima (2008), Hogan and Matricardi (2022)).

The extent to which errors in radiative fluxes or heating rates affect the outcome of atmospheric simulations may be very application specific. Large-scale climate simulations, in which small radiative imbalances due to enhanced concentrations of greenhouse gases can accumulate over long time periods, are likely sensitive to small errors in radiative fluxes that may arise when approximating the spectral integration (Chung & Soden, 2015; Zhang & Huang, 2014). The sensitivity of cloud-resolving simulations such as large-eddy simulations (LES) is likely much smaller because these simulations have short integration times, typically one diurnal cycle up to a couple of days (e.g., Gristey et al., 2020; Seifert et al., 2015). Furthermore, in marine LES cases, sea surface temperatures or surface heat fluxes are often fixed and thus not even coupled to the surface irradiance (Klinger et al., 2017; Wing et al., 2018). Pincus and Stevens (2009) have shown that even relatively large random spatiotemporal noise in radiative heating rates, arising from their Monte Carlo approach to spectral integration, does not significantly affect the cloud and turbulence statistics of a stratocumulus LES.

In this study, we further explore the link between radiative metrics and simulation accuracy using three different numerical experiments: (a) radiative-convective equilibrium (RCE), (b) shallow convection over the tropical ocean and (c) shallow convection over land. Our focus here is on LES, where we expect a low sensitivity of simulation accuracy to radiative accuracy and thus a large potential for speeding up simulations by reducing the size of the *k*-distributions. LES are typically used to compute the statistics of turbulent atmospheric flows under idealized conditions, so we are concerned with the mean properties of the simulations rather than specific flow features. To allow radiative transfer computations with different degrees of accuracy, we first create smaller sets of *g*-points from an existing *k*-distribution by repeatedly combining adjacent *g*-points while minimizing a cost function composed of radiative metrics. A number of reduced *k*-distributions are then implemented in the simulations, where we study either the long-term mean cloud properties and state of the atmosphere (RCE), or the transient behavior of the shallow cumulus cloud fields. Whereas Pincus and Stevens (2009) studied the effects of spectral noise at short spatiotemporal scales, our focus here is on the impact of systematic biases in radiative heating rates resulting from the reduction in the spectral detail of the *k*-distributions. By comparing simulations performed with *k*-distributions of different accuracies, we can better understand where the optimal balance lies between computational performance and radiative accuracy for cloud-resolving LES.

In Section 2, we describe the optimization algorithm used to produce smaller *k*-distributions as well as the resulting *k*-distributions used further in this study. The numerical LES experiments are described in Section 3. The results are shown in Section 4 and in Section 5 we provide a discussion and short conclusions.

## 2. Reducing the Number of *g*-Points

We generate smaller sets of *g*-points to lower the spectral detail in gaseous optical properties resolved by the radiative transfer scheme and thus its accuracy. Instead of developing *k*-distributions from scratch (e.g., Hogan & Matricardi, 2022; Pincus et al., 2019; Sekiguchi & Nakajima, 2008), we create smaller *k*-distributions by combining adjacent *g*-points (Appendix A1), starting from the *k*-distributions of Pincus et al. (2019). This procedure of combining *g*-points is similar to how RRTMG was constructed from its predecessor RRTM (not well documented, but an overview of RRTM and RRTMG is given by Iacono et al. (2008)). Rather than manually selecting which *g*-points are combined, we use an exhaustive and greedy optimization approach to iteratively reduce the number of *g*-points. At each iteration, the cost function (Appendix A2) is computed for every possible *g*-point merging and the merging which increases the costs least is chosen for the next *k*-distribution with one *g*-point fewer. This procedure is repeated until no more *g*-point combinations are possible, that is, one *g*-point remains in each spectral band. Cloud optical properties are computed per spectral band in RRTMGP and therefore unaffected

**Table 1**
*Overview of the Radiative Metrics (Downwelling Surface Irradiance, Upwelling Top-Of-Atmosphere (TOA) Irradiance, Atmospheric Heating Rates) Used in the Three Cost Functions (cf) Are Explored in This Study*

| | Surface irradiance | TOA irradiance | Heating rates |
|---|---|---|---|
| cf1 | | | X |
| cf2 | X | X | X |
| cf3 | X | | X (>100 hPa) |

by our optimization, because we retain the same bands as RRTMGP and only combine *g*-points within spectral bands.

An advantage of our optimization procedure is its simplicity and computational efficiency. However, we can not add spectral detail beyond what is contained in the reference k-distributions of RRTMGP and may not produce the most optimal *k*-distribution because the algorithm simply searches the local minimum at each iteration. Our reduced sets of *g*-points are nevertheless useful to explore the link between radiative and simulation accuracy, which is the focus of this study. Producing new *k*-distributions directly from high-resolution spectroscopic databases (e.g., Rothman et al., 2005) likely enables a more efficient distribution of *g*-points and thus a smaller *k*-distribution to achieve the same accuracy (see e.g., Hogan & Matricardi, 2022; Sekiguchi & Nakajima, 2008). Finding the most optimal *k*-distribution, however, is beyond the aim of this study.

In this study, we explore three cost functions (Table 1) that are designed to minimize normalized root mean squared errors of a set of radiative metrics (e.g., surface irradiance, upwelling TOA irradiance, heating rates) with respect to line-by-line computations (LBLRTM; Clough et al., 2005). The first cost function (cf1) is motivated by simulations with fixed surface temperatures or heat fluxes (e.g., marine cases; Siebesma et al., 2003; van Zanten et al., 2011; Wing et al., 2018), and therefore accounts only for errors in atmospheric heating rates. The second cost function (cf2) is designed for simulations with a stronger surface coupling or simulations with long integration times (weeks, months), in which the net radiation balance of the atmosphere plays a larger role. This cost function optimizes for atmospheric heating rates as well as surface and TOA irradiances, the same radiative metrics used by Hogan and Matricardi (2022) to produce new *k*-distribution directly from line-by-line absorption data. The last cost function (cf3) is aimed at typical LES experiments with a limited vertical extent and therefore optimizes only for surface irradiance and tropospheric heating rates (>100 hPa).

Ideally, the optimization of *k*-distributions is directly based on interactive simulations of the atmosphere. Instead of relying solely on radiative metrics, cost functions would then be additionally composed of metrics based on for example, cloud statistics or thermodynamic quantities such as temperature and humidity. However, this would be computationally extremely expensive since it requires a new simulation for each possible combination of *g*-points. Our approach therefore still relies on radiative metrics, chosen in consideration of simulation accuracy for different types of LES simulations.

We optimize of the set of 42 Garand et al. (2001) clear-sky atmospheres, consistent with how the *k*-distributions of RRTMGP were developed. These atmospheric profiles cover a wide range of atmospheric conditions for temperature, water vapor, ozone as several other gases, from 1013.25 hPa up to 0.1 hPa, with constant concentrations of $CO_2$, $O_2$, and $N_2$. The same set of profiles was used by Pincus et al. (2019) construct their *k*-distributions, but with some data augmentation to also take the radiative forcing of several greenhouse gases into account. The 100 atmospheric profiles chosen by the Radiative Forcing Model Intercomparison Project (RFMIP; Pincus et al., 2016) provide out-of-sample data to evaluate the cost functions based on the radiative metrics. During the optimization and evaluation, radiative fluxes are computed using a two-stream method for shortwave radiation and a no-scattering solution with three Gaussian quadrature angles for longwave radiation (Pincus et al., 2019).

The progressive changes in costs during the *g*-point reduction are shown in Figure 1. The initial costs and the change therein with each iteration step, that is, one combination of adjacent *g*-points, strongly depend on the chosen radiative metrics (Figure 1). The costs initially decrease after each iteration step, suggesting that the first couple of reduced *k*-distributions are slightly more accurate than the original *k*-distribution. After this initial decrease, the costs remain relatively constant for ∼100 iterations, after which they start increasing rapidly (note the logarithmic vertical axis). The initial insensitivity of the costs to the number of *g*-points is likely because of the fixed spectral resolution that was used to generate the *k*-distributions of RRTMGP, meaning that these *k*-distributions already have some redundant spectral detail that does not contribute significantly to the accuracy of RRTMGP. Moreover, we relieved some of the constraints used in the development of RRTMGP, such as the need to provide accurate radiative forcings due to increased greenhouse gas concentrations. The relative errors of most of the *k*-distributions, including the initial *k*-distributions, are higher in the out-of-sample evaluation with the RFMIP profiles than with the Garand profiles (Figure 1). However, the costs computed from either the Garand or the

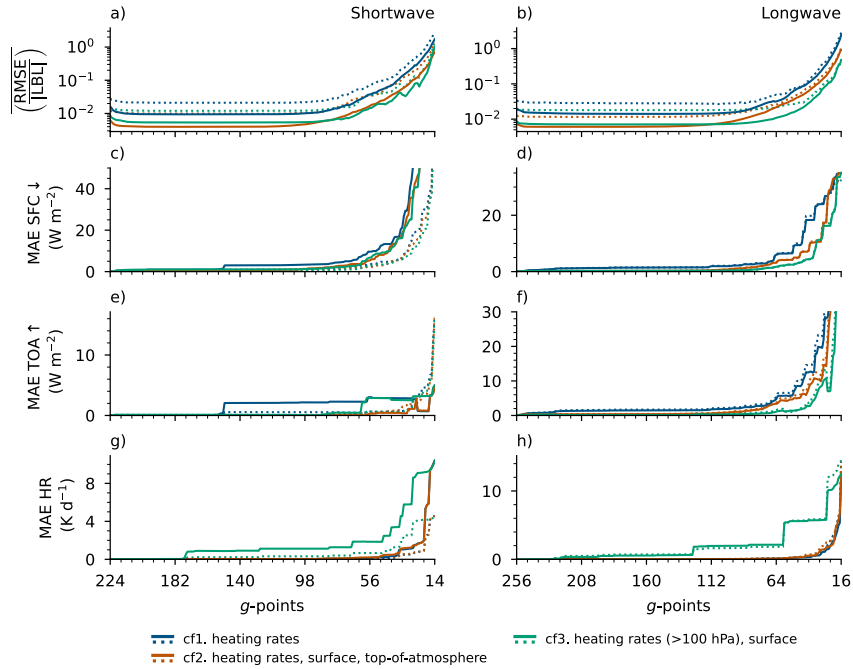


**Figure 1.** Costs averaged over each radiative metric (see Table 1) (a, b), mean absolute error (MAE) of downwelling surface irradiance (c, d), MAE of upwelling top-of-atmosphere irradiance (e, f), and MAE of atmospheric heating rates (g, h), as function of the remaining number of shortwave (left) or longwave (right) *g*-points for each cost function. Solid lines are computed with the 42 Garand et al. (2001) profiles used for the optimization, dotted lines with the 100 Radiative Forcing Model Intercomparison Project (Pincus et al., 2016) profiles as out-of-sample evaluation.

RFMIP profiles show a similar trend, indicating that the optimization results can be generalized beyond the Garand atmospheres.

Including surface and TOA irradiance in the cost function generally improves the accuracy of these radiative fluxes, but slightly degrades the accuracy of the atmospheric heating rates (Figure 1). Optimizing for only surface irradiance and tropospheric heating rates also improves the TOA irradiance in the longwave spectrum, but results in worse TOA irradiances in the shortwave spectrum. The heating rate errors are computed from the full vertical extent of the RFMIP and Garand profiles, and consequently larger for the cost function that only considers tropospheric heating rates.

## 3. Numerical Experiments

To study the sensitivity of simulation accuracy to radiative accuracy, we perform a number of LES using the MicroHH (van Heerwaarden et al., 2017) model coupled to a C++ front-end of RTE + RRTMGP for radiative transfer. Based on the results of the optimization procedure (Section 2), a number of reduced longwave or shortwave *k*-distributions are chosen from each cost function. Simulations performed with the *k*-distributions (224 shortwave, 256 longwave *g*-points) provided by Pincus et al. (2019) serve as reference.

We use three LES experiments that differ in initial and background conditions as well as variables and statistics of interest. The first experiment is the radiative-convective equilibrium `(RCE)`, a slowly developing equilibrium between radiative cooling and (deep) convection, where our main focus is on capturing the mean state of the atmosphere. The simulations follow the RCE Model Intercomparison Project (RCEMIP; Wing et al., 2018, 2020) specifications for LES, with a horizontal domain of $48 \times 48$ km$^2$ a horizontal resolution of $200 \times 200$ m$^2$ and a fixed sea surface temperature (SST) of 300 K. The RCE simulations are run for 50 days and analyzed based on hourly output of the last 10 days. We do not use *k*-distributions produced with cost function 3 (cf3; Table 1) in the RCE experiment since its domain extends far above the troposphere. Since the SST is fixed, any improvements in surface irradiance by including it in cost function 2 will not directly impact the simulations. However, adding multiple terms to the cost function slightly deteriorates the accuracy of the heating rates (Figure 1) after a given number of iterations in the optimization, which may affect the RCE simulations.

The second and third experiments focus more on the shorter-term (e.g., diurnal) variability. The second experiment (RICO) is based on the Rain in Cumulus over the Ocean (Rauber et al., 2007) case described by van Zanten et al. (2011), which has a fixed SST of 299.8 K. However, we use a domain of $48 \times 48 \times 6$ km$^3$, a resolution of $100 \times 100 \times 20$ m$^3$, a longer simulation period of 30 hr and we neglect the 2.5 K d$^{-1}$ large scale cooling originally prescribed by van Zanten et al. (2011) because we use interactive radiative transfer, comparable to the `irad-zero` experiment of Seifert et al. (2015). The third experiment (`Cabauw`) is based on a case developed and thoroughly compared to observations by Tijhuis et al. (2022); a summer day (15 August 2016) in `Cabauw`, the Netherlands, with shallow cumulus clouds developing in the afternoon. The Cabauw simulations are run from 6 to 18 UTC (8–20 local time), with a domain of $24 \times 24 \times 8.5$ km$^3$, a horizontal resolution of $50 \times 50$ m$^2$ and a stretched vertical grid from 20 m at the surface to 95 m near the domain top. Initial and boundary conditions are obtained from the ERA5 reanalysis (Hersbach et al., 2020).

To account for radiative effects such as ozone absorption above the shallow domains of the `Cabauw` and `RICO` simulations, we first compute radiative fluxes based on one-dimensional background profiles of temperature, water vapor, ozone, and other gases. The downwelling radiative fluxes at the domain top are then used as boundary conditions for the radiative transfer computations in the simulation domain. The background profile of the `Cabauw` simulations is obtained from the `ERA5` reanalysis, the background profile of the `RICO` simulations is based on the `RCEMIP` specifications.

In the `RCE` experiment, we parametrize microphysics using the six-class microphysics scheme of Tomita (2008) and the sedimentation parametrization of Stevens and Seifert (2008). In the `Cabauw` and `RICO` experiments, we use the two-moment warm cloud parametrization of Seifert and Beheng (2006) because clouds are too warm for ice to develop.

To understand how radiative accuracy propagates to simulation accuracy, we first need to define the latter. However, choosing appropriate metrics to assess simulation accuracy is challenging. For example, Pincus and Stevens (2009) argued that random radiative heating rates errors introduced by Monte Carlo spectral integration are acceptable as long as the most energetic eddies are unaffected. Since our focus is on LES of convective clouds, we choose to primarily compare statistical cloud properties between simulations. For the `RCE` simulations, we therefore compute mean liquid and ice water paths (LWPs, IWPs), liquid water and ice cloud covers ($cc_{liquid}$, $cc_{ice}$), and mean cloud radiative effect (CRE) over the last 10 days of each simulation. The CRE serves as an integral measure of the accuracy of the simulated cloud properties because it depends on LWP, IWP, $cc_{liquid}$, and $cc_{ice}$. As we do not modify the spectral bands of RRTMGP, the per-band defined cloud optical properties are not changed and do not directly contribute to any biases in CRE. In addition to cloud properties, we examine more convective metrics such as vertical turbulent temperature fluxes and vertical velocity variances. For the simulations of the `RICO` and `Cabauw` experiments we mostly use a subset of the quantities we consider in the `RCE` simulation. As the focus in these experiments is on the shorter-term variability, we compare time series rather than temporal averages. For the `RICO` simulations, we compare time series of mean LWP and cloud cover, precipitation statistics, and vertical velocities. For the `Cabauw` simulations, we consider mean LWP and cloud cover, as well as surface latent and sensible heat fluxes.

## 4. Spectral Accuracy in Large-Eddy Simulations

### 4.1. Heating Rates and Radiative-Convective Equilibrium Solutions

For the `RCE` simulations, we first take five reduced *k*-distributions each from cost functions 1 and 2 for both longwave and shortwave radiation and perform a simulation with each reduced *k*-distribution. We select the *k*-distributions with the lowest costs and the smallest *k*-distributions whose costs do not exceed that of the initial *k*-distribution. Additionally, we use the *k*-distributions after 100, 200, and 220 iterations (156, 56, and 32 *g*-points, respectively) for longwave and after 100, 175, and 190 iterations (124, 49, and 34 *g*-points, respectively) for shortwave radiation. These *k*-distributions at a fixed number of iterations are chosen as exploration and help to assess to what extent the specific radiative metrics that are optimized for affect simulation accuracy after a given number of iterations.

Reducing the number of *g*-points results in larger radiative heating rate biases and larger deviations in cloud statistics from the `Reference` simulation (Figures 2a–2d, e–h). The accuracy of the mean shortwave heating rates is generally affected more than the accuracy of the mean longwave heating rates. We hypothesize that this

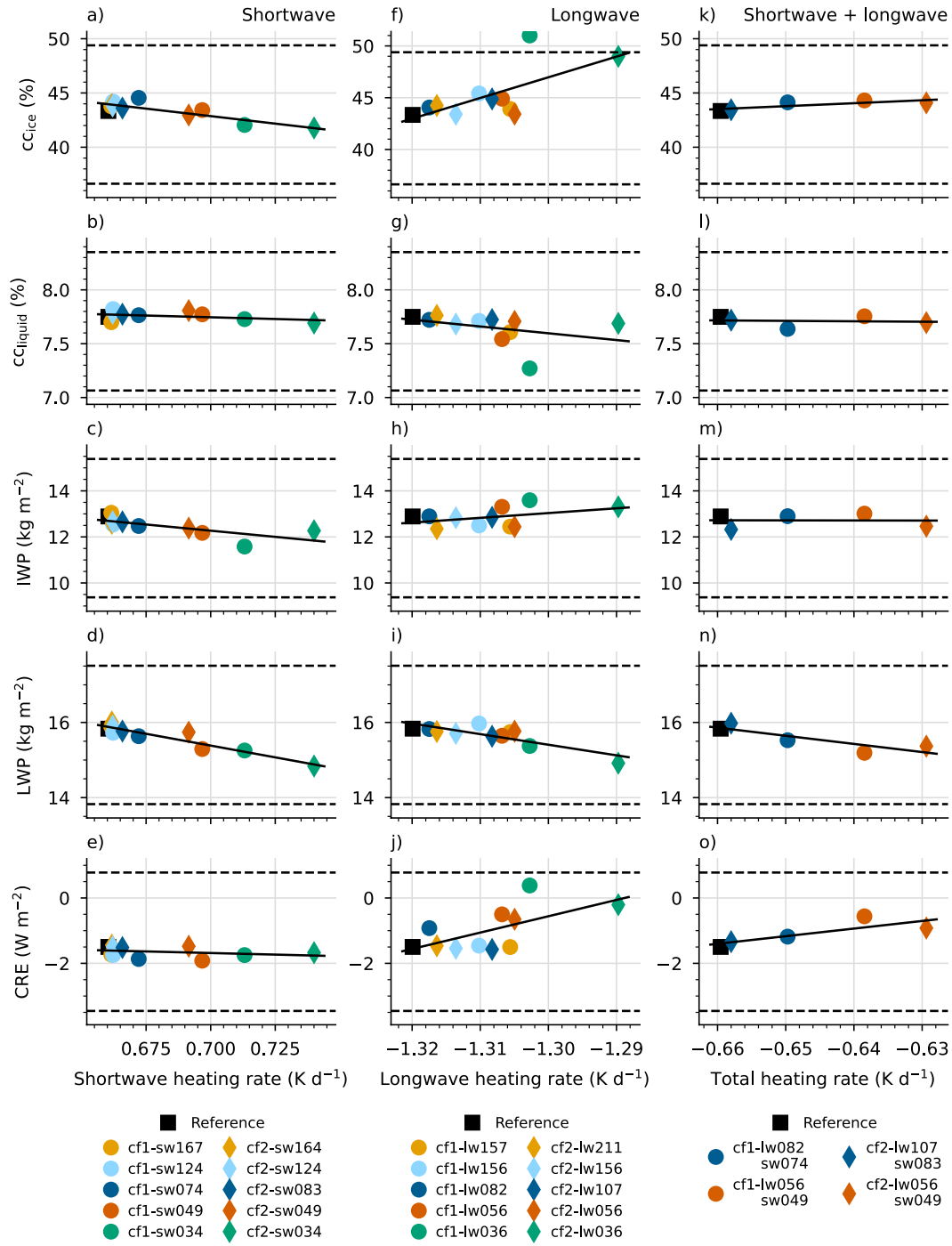


**Figure 2.** Scatter plots of ice cloud cover ($cc_{ice}$; a, f, k), liquid water cloud cover ($cc_{liquid}$; b, g, l), ice water path (IWP; c, h, m), liquid water path (LWP; d, i, n), and cloud radiative effect (CRE; e, j, o) against shortwave (a–e), longwave (f–j) and total (k–o) tropospheric (<15.5 km) radiative heating rates for all `radiative-convective equilibrium` simulations with reduced *k*-distributions for shortwave radiation (a–e), longwave (f–j) radiation, or both (k–o). CRE shows the combined shortwave and longwave effect of clouds on the upwelling top-of-atmosphere irradiance, negative values indicate less radiation escaping to space. All metrics are averaged over the last 10 days (day 40–50) of each simulation. The dashed horizontal lines show the 25th–75th percentile range of Reference to indicate the typical temporal variability of the cloud statistics. Linear trendlines (solid lines) are shown for visual guidance.

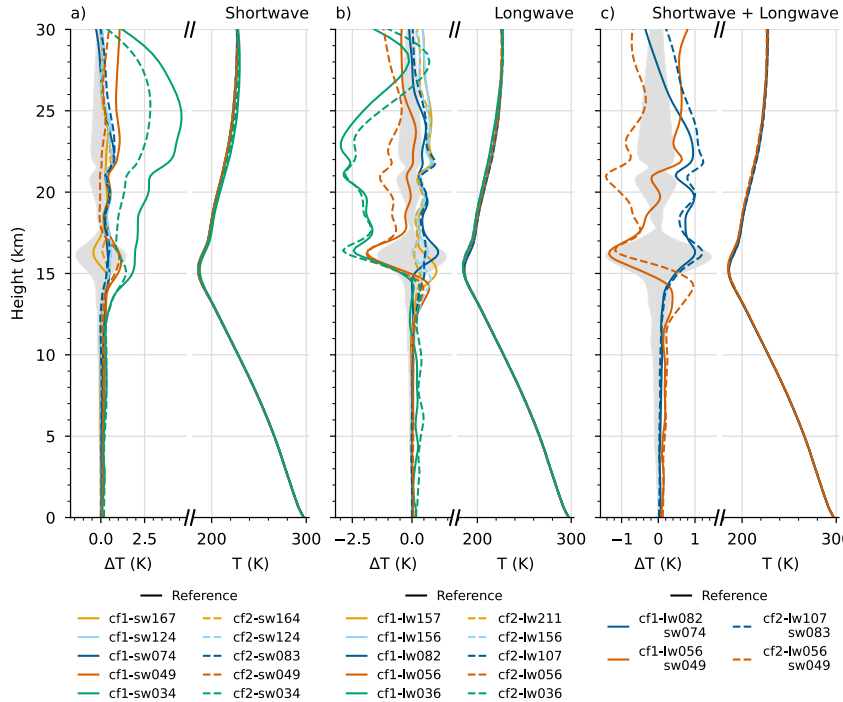


**Figure 3.** Vertical profiles, averaged over the last 10 days, of absolute temperatures ($T$) and deviations thereof ($\Delta T$) from `Reference` for all `radiative-convective equilibrium` simulations with reduced $k$-distributions for (a) shortwave, (b) longwave, and (c) both shortwave and longwave. The shaded area shows the 5–95th percentile range of the temporal variability, based only on the `Reference` simulation.

is because in the shortwave spectrum only the absorption is affected when the number of $g$ is reduced, whereas in the longwave spectrum both absorption and emission are affected, which leads to compensating errors. Additionally, any deviation in longwave heating rates due to a reduced number of $g$-points may be partly compensated by differences in the vertical temperature profile arising from these deviations. Simulations with reduced shortwave $k$-distributions show strong correlations of mean shortwave radiative heating rates with $cc_{ice}$ (correlation coefficient $\rho = -0.86$), IWP ($\rho = -0.73$), and LWP ($\rho = -0.94$), whereas simulations with reduced longwave $k$-distributions show strong correlations of mean longwave radiative heating rates with $cc_{ice}$ ($\rho = 0.68$), LWP ($\rho = -0.83$) and CRE ($\rho = -0.63$). If we only compare the simulations with the three largest $k$-distributions, however, the correlation between deviations in heating rates and deviations in cloud properties is much less clear. Except with the smallest $k$-distributions (`-sw034, -lw036`), differences in cloud properties between the simulations are well within the temporal variability of `Reference`.

Among the smallest shortwave and longwave $k$-distributions, cost function 2 consistently produces the largest heating rate errors, consistent with a cost function that minimizes errors in both heating rates and boundary fluxes. However, neither cost function seems to produce consistently more accurate $k$-distributions in terms of cloud properties than the other, which suggests a relatively small sensitivity of simulation accuracy to the chosen cost function. In simulations with interactive surface heat fluxes, rather than a fixed SST, we may expect a larger sensitivity to including surface irradiance in the cost function.

We consider a detailed analysis of the physical mechanisms that relate heating rate errors to differences in cloud properties out of scope. Nevertheless, it is important to note that causal relationships between radiative heating rates and cloud properties can be bidirectional: radiative heating affects clouds formation by modifying the vertical temperature distribution, while clouds modify the vertical structure of radiative heating by locally enhancing the absorptivity and emissivity of the atmosphere. For example, the correlation between longwave heating rates and $cc_{ice}$ (Figure 2f) is likely driven to a large extent by the enhanced trapping of longwave radiation in the troposphere in simulations with higher mean ice cloud covers.

To further compare the simulations, we examine vertical profiles of absolute temperature $T$ and specific humidity $q_t$ (Figures 3 and 4). Errors in the $T$ and $q_t$ profiles with respect to `Reference` are mostly about two orders of

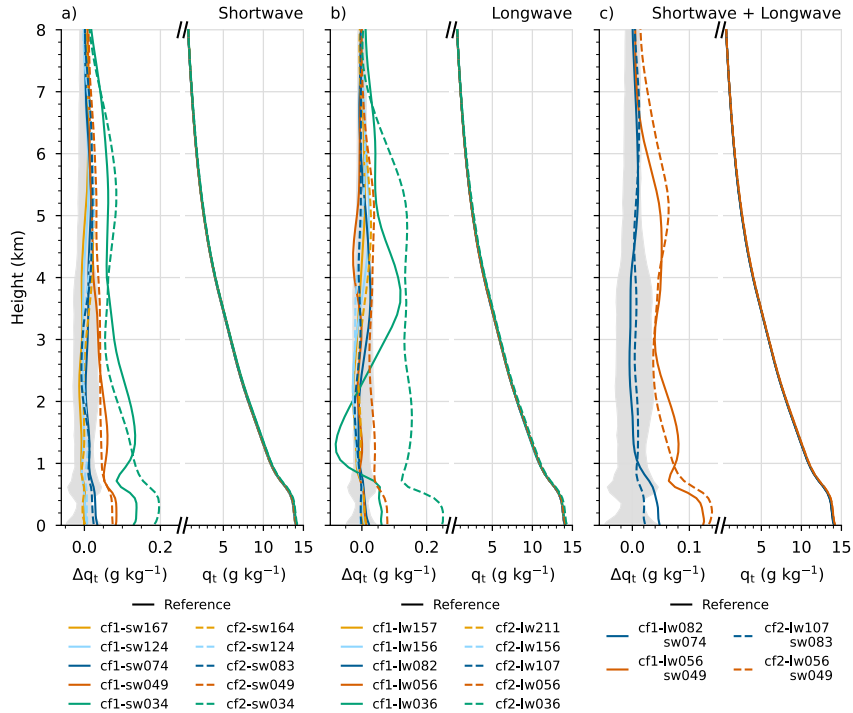


**Figure 4.** Vertical profiles, averaged over the last 10 days, of specific humidity ($qt$) and deviations thereof ($\Delta qt$) from `Reference` for all `radiative-convective equilibrium` simulations with reduced $k$-distributions for (a) shortwave, (b) longwave, (c) and both shortwave and longwave. The shaded area shows the 5–95th percentile range of the temporal variability, based only on the `Reference` simulation.

magnitude smaller than their means. In the lower atmosphere (below 12 km), only the simulations with the smallest $k$-distributions (`-sw034, -lw036`) have temperature and humidity errors exceeding 0.3 K and 0.1 g kg$^{-1}$, respectively. In the upper atmosphere, temperature errors are up to 4.6 K with the smallest $k$-distributions and errors in relative humidity (not shown) are up to about 20%. In RCE, however, stratospheric temperature and humidity errors do not significantly impact the dynamics of the troposphere and are therefore not considered relevant for the metrics, that is, cloud cover and water path, we use to assess simulation accuracy. Since the focus of this study is on producing accurate cloud statistics, we mainly consider the lower atmosphere.

To study the combined effect of lowering the accuracy of shortwave and longwave computations, we perform four additional simulations with the second and third smallest longwave and shortwave $k$-distributions of cost functions 1 and 2 (Figures 2i–2l, 3c, 4c$^{2i-2l}$). Deviations in cloud properties are similar to the deviations found in the simulations where either the shortwave or the longwave $k$-distribution was reduced. However, the vertical profiles of $T$ and $q_t$ show larger errors than the corresponding simulations with only one reduced $k$-distribution, which could be expected from Figures 2a–2h: tropospheric shortwave and longwave heating rates both increase (i.e., more warming, less cooling) when the number of $g$-points in the respective $k$-distributions is reduced, so the impact of both on the $T$ and $q_t$ profiles add up. In the troposphere, only `cf1-lw082-sw074` and `cf2-lw107-sw083` are still within the 5–95th percentile range of `Reference` and in the stratosphere, all four simulations are generally outside this range. The simulations using $k$-distributions based on cost function 2 produce lower cloud condensates, lower vertical velocity variances and a weaker vertical liquid water vertical potential temperature flux in the upper troposphere (8–12 km) (Figure 5). This indicates a minor degradation in simulation accuracy to including surface and TOA irradiance to the cost function rather than optimizing solely for atmospheric heating rates: due to their fixed SST, the `RCE` the simulations do not respond to errors in surface irradiance.

### 4.2. Shorter-Term Impact of Radiative Accuracy

In contrast to the `RCE` experiment, our focus in the `RICO` and `Cabauw` experiments is on accurately capturing the transient behavior of the atmosphere. In both experiments, we use the combined longwave and

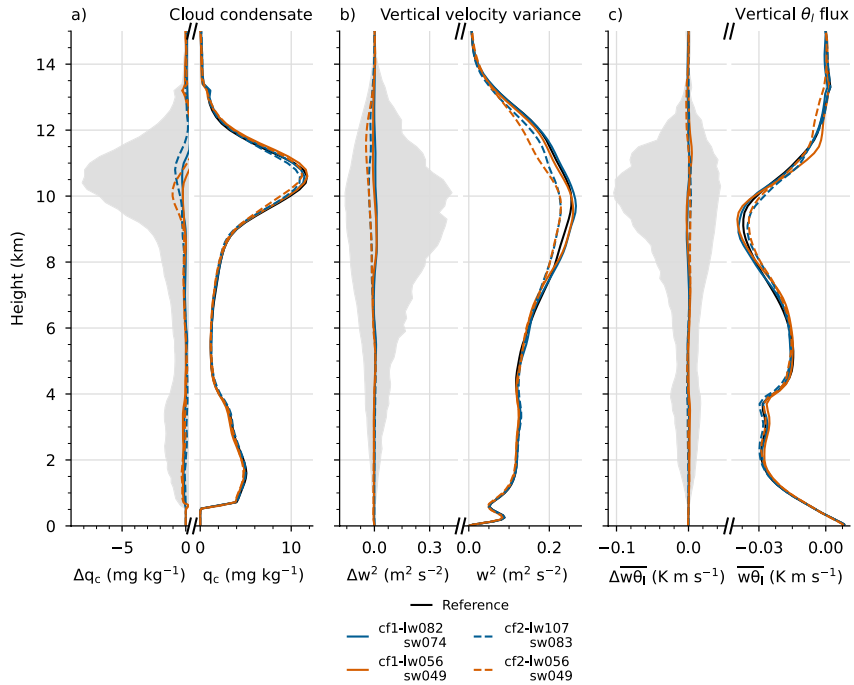


**Figure 5.** Vertical profiles, averaged over the last 10 days, of (a) total cloud condensate (liquid water and ice) ($q_c$), (b) vertical velocity variance ($w^2$), (c) vertical liquid water potential temperature flux $\left(\overline{w\theta_l}\right)$, and respective deviations ($\Delta q_c$, $\Delta w^2$, $\Delta\overline{w\theta_l}$) from `Reference` for all `radiative-convective equilibrium` simulations with reduced *k*-distributions for both shortwave and longwave. The shaded area shows the 5–95th percentile range of the temporal variability, based only on the `Reference` simulation.

shortwave *k*-distributions (`cf1-lw082-sw074`, `cf1-lw056-sw049`, `cf2-lw107-sw083`, `cf2-lw056-sw049`), and additionally two sets of *k*-distributions from cost function 3 (surface irradiance and tropospheric heating rates), because in both experiments the whole dynamical domain is within the troposphere (>100 hPa),

In the `RICO` simulations with reduced *k*-distributions, simulated cloud properties, rain rates, and vertical velocity variances generally follow the same trend as in the `Reference` simulation. Also, temporal fluctuations within each simulation are almost an order of magnitude larger than mean differences between the simulations. For example, the largest deviation in mean rain rate from `Reference` is 4.8 g m$^{-2}$ hr$^{-1}$ (`cf3-lw076-sw066`), while temporal fluctuations are over 50 g m$^{-2}$ hr$^{-1}$. In Section 5, we further discuss the interpretation of differences in cloud and rain properties between simulations. Mean surface irradiances in the `RICO` simulations differ up to 3.5 W m$^{-2}$ for shortwave and between 7.0 W m$^{-2}$ for longwave radiation, but note these surface irradiance errors do not directly impact cloud evolution in these simulations due to the fixed SST.

Interestingly, most simulations have peaks in the precipitation rate over 25 g m$^{-2}$ hr$^{-1}$ higher than the highest precipitation rate in `Reference` and half have peaks more than twice as high as the highest precipitation rate in `Reference` (≈50 g m$^{-2}$ hr$^{-1}$). Whether this is an effect of the reduced accuracy in radiative heating rates, or an artifact of potentially having a too small domain size or too short simulation period, is not clear. Using comparable simulations of `RICO`, but with a slightly larger domain of 51.2 × 51.2 × 5 km$^3$, a resolution of 25 × 25 × 25 m$^3$ and varying cloud droplet densities, Seifert et al. (2015) already showed that with interactive radiation their simulations may take over 30 hr to reach a quasi-equilibrium and continue to have temporal fluctuations up to about 50 g m$^{-2}$ hr$^{-1}$. The 30 hr simulation period together with the 48 × 48 km$^2$ horizontal domain used in our `RICO` simulations may therefore be insufficient to have fully reached statistical convergence.

We find similar results for the `Cabauw` experiment: despite mean shortwave and longwave irradiance errors of up to −5.5 and 4.8 W m$^{-2}$, respectively, deviations in cloud properties and surface heat fluxes between simulations with reduced *k*-distributions and the `Reference` simulations are generally small compared to temporal fluctuations (Figure 7). Again, these short-term fluctuations are presumably the result of not yet reaching statistical

convergence with the 24 × 24 km$^2$ horizontal domain used in the `Cabauw` simulations. Nevertheless, there is a small bias as simulations with larger irradiance errors tend to produce fewer and smaller clouds: averaged between 9:30 and 13:30 UTC, the difference in cloud cover and LWP between `Reference` and `cf3-lw056-sw049` are about 1.2% and 1 g m$^{-2}$, respectively, which is approximately of the same order as the largest short term fluctuations in the simulations.

Overall, all six combinations of reduced longwave and shortwave *k*-distributions produce simulations with relatively small mean deviations in cloud properties, precipitation amounts and surface heat fluxes compared to temporal variability. If highly accurate surface irradiance predictions are required explicitly, the three smallest longwave and shortwave *k*-distributions tested here would be less suitable. However, the accuracy of the radiative fluxes in the `RICO` and `Cabauw` simulations may even be further improved by prescribing more accurate incoming fluxes at the top of the domain (6 and 8.5 km, respectively) to reduce errors originating above the dynamical domain.

## 5. Radiation Errors in Context

In this study, we reduced the spectral discretization of clear-sky radiative transfer calculations to explore how the spectral detail of radiative transfer computations affects cloud-resolving LES. Starting from the *k*-distributions of Pincus et al. (2019), we first used an optimization algorithm that repeatedly combines adjacent *g*-points while minimizing errors in radiative fluxes and heating rates. For three LES experiments with different cloud—radiation coupling pathways, we then performed LES with a couple of reduced *k*-distributions to study how radiative accuracy propagates to simulation accuracy: deep (`RCE`) and shallow (`RICO`) convection over the tropical ocean, and shallow convection over land (`Cabauw`) in the mid-latitude summer. The majority of the evaluated *k*-distributions did not cause major biases in the simulations, which suggests that even relatively large systematic errors in spectral integration do not have a significant error on cloud-resolving simulations, especially on short time scales. In `RCE`, where spectral integration errors can accumulate over longer time-scales, we do find a relatively small degradation in the accuracy of simulated cloud properties as the accuracy of radiative heating rates decreases. However, the impact of the reduced spectral accuracy on the `RCE` simulations may be dampened by the use of a prescribed SST following the specifications of Wing et al. (2018) because it does not allow surface irradiance errors to accumulate.

Whereas evaluating radiative accuracy is relatively straightforward using line-by-line computations of radiative fluxes and heating rates, evaluating the simulations with reduced *k*-distributions requires choosing appropriate metrics for simulation accuracy. Our focus is predominantly on the simulated cloud field properties, but we additionally compare precipitation statistics (`RICO`) and surface heat fluxes (`Cabauw`). The main difficulty is then to establish what deviations from a reference simulation are within acceptable limits. This is the case especially when no observations are available for validation (e.g., `RCE, RICO`) or when the reference simulations already deviates quite strongly from observation, which is not uncommon for realistic LES (e.g., Brown et al., 2002; Duynkerke et al., 2004; Gustafson et al., 2020; Tijhuis et al., 2022). In this study, we have used the temporal variability within the `Reference` simulations to put the mean differences between simulations into context. In simulations with 3–4 times smaller *k*-distributions, mean deviations in cloud properties remain relatively small compared to the temporal variability. However, the large temporal variability in our simulations (e.g., Figure 6), presumably a consequence of the relative small horizontal domains, also limits the interpretability of our results. In future work, our reduced *k*-distributions should therefore be evaluated in simulations with significantly larger horizontal domain sizes to improve statistical convergence. Given that the magnitude of the temporal variability can largely depend on the chosen domain size, however, comparing mean biases and temporal fluctuations in cloud properties may then still not be the most optimal metric for evaluating *k*-distributions.

Multiple model intercomparison studies (Siebesma et al., 2003; van Zanten et al., 2011; Wing et al., 2018, 2020) have shown that different LES models, which have varying numerical implementations of for example, advection, diffusion and microphysics, may produce a large spread in the predicted evolution of the atmosphere, often with no clear indication of what model is most accurate. Even with the smallest *k*-distributions (`-sw034, -lw036`), deviations in the vertical profiles of $T$ and $q_t$ with respect to `Reference` are mostly within the uncertainty range of the RCEMIP ensemble (Wing et al., 2020), indicating that the sensitivity to the spectral discretization may be rather low compared to the sensitivity of simulations to other parametrizations. Differences in mean cloud properties between our `RCE` simulations are also smaller than the ensemble spread reported by Wing et al. (2020). Furthermore, in comparable simulations of RICO, but without interactive radiative transfer, Seifert et al. (2015) noted that just changing the random seed may significantly delay the onset of precipitation and the

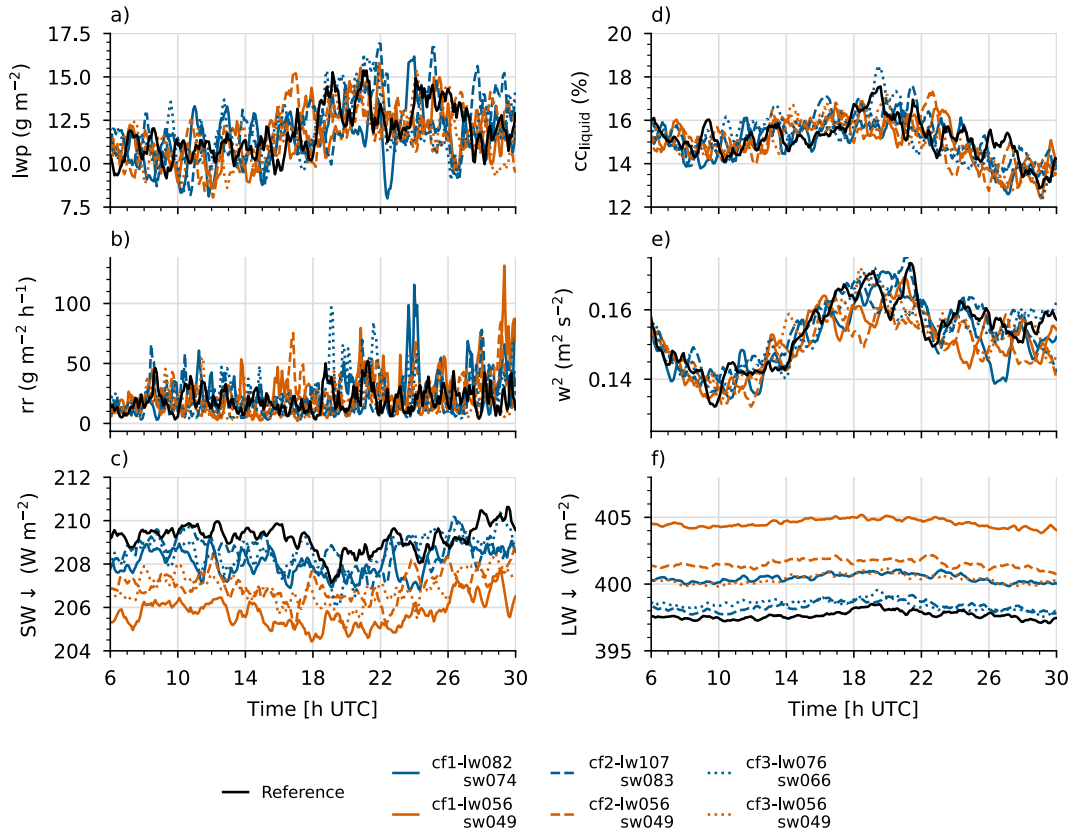


**Figure 6.** Time series of (a) liquid water path (LWP), (b) rain rate (rr), (c) Shortwave surface irradiance (SW ↓), (d) liquid water cloud cover ($cc_{liquid}$), (e) vertical velocity variance ($w^2$) and (f) longwave surface irradiance (LW ↓) for the reference RICO simulation and the six RICO simulations with reduced longwave and shortwave *k*-distributions. $w^2$ is taken at $z = 200$ m, which is the height with the highest $w^2$ within the subcloud layer. The first 6 hr are considered spin-up time to allow the turbulence to stabilize sufficiently (see e.g., van Zanten et al., 2011).

transition to a quasi-stationary precipitation regime by several hours. We performed a small sensitivity test (not shown) by repeating the reference simulation of each experiment with fifth order interpolation in the advection scheme, instead of 3rd (`RCE`) or fourth (`RICO, Cabauw`) order interpolation, and found that changing the advection scheme can have a substantially larger impact on simulated cloud properties than using the smallest *k*-distributions tested in this study. Variations in cloud and rain properties due to reduced *k*-distributions may thus be significantly smaller than variations due to other numerical choices. However, this does not imply that the sensitivity to any other numerical implementations provides an upper bound for what errors in the simulations should be tolerated.

Based on three numerical experiments with either deep or shallow convection, our results show potential for a strong reduction in the number of *g*-points in cloud-resolving LES, which reduces computational costs or allows more frequent radiative transfer computations. However, to further investigate the robustness of our results, the impact of the reduced k-distributions on simulated cloud properties should be evaluated on a more diverse ensemble of numerical experiments, for example, spanning a wider range of cloud types such as stratocumulus, fogs, and cirrus. Moreover, the dominant physical mechanisms that propagate errors in radiative fluxes and heating rates to errors in simulated cloud properties should be better understood.

## Appendix A: Optimization Method

### A1. Combining *g*-Points

Two *g*-points within the same band are combined by computing the weighted averaged absorption ($k_{abs}$) and rayleigh scattering ($k_{rayleigh}$) coefficients

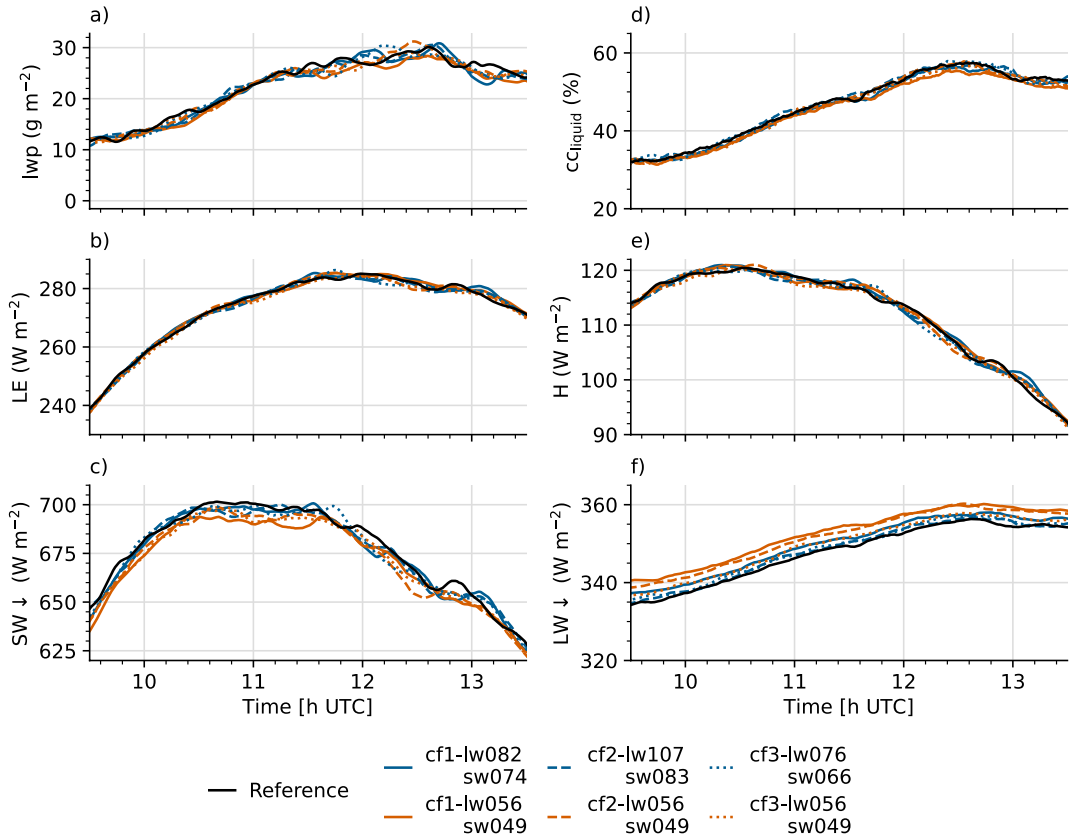


**Figure 7.** Time series from 9:30 UTC to 13:30 UTC of (a) liquid water path, (b) latent heat flux (LE), (c) shortwave surface irradiance (SW ↓), (d) liquid water cloud cover ($cc_{liquid}$), (e) sensible heat flux (H) and (f) longwave surface irradiance (LW ↓) the reference Cabauw simulation and the six Cabauw simulations with reduced longwave and shortwave *k*-distributions.

$$k_{ij} = \frac{k_i w_i + k_j w_j}{w_i + w_j},\ k \in \left[k_{rayl}, k_{abs}\right],$$

and adding the Planck fractions ($f$), solar source terms ($S$) and $g$-point weights $w$ added:

$$f_{ij} = f_i + f_j,$$

$$S_{ij} = S_i + S_j,$$

$$w_{ij} = w_i + w_j.$$

Here, subscripts $i$ and $j$ indicate the $i$th and $j$th $g$-points within a spectral band and in our optimization method $j = i + 1$ because we only combine adjacent $g$-points. $w$ which is the fraction of the cumulative probability function $g(k_{abs})$ represented by each $g$-point. The Planck fraction is the fraction of the band's Planck source function at each $g$-point.

### A2. Cost Function

The accuracy of each *k*-distribution is assessed by computing a predefined cost function $C$,

$$C = \frac{1}{N_{qty}} \sum_{i=0}^{N_{qty}} \frac{1}{N_{lev}(i)} \sum_{l=0}^{N_{lev}(i)} \frac{\sqrt{\frac{1}{N_{col}} \sum_{c=0}^{N_{col}} \left(F_{c,l}^{i} - \hat{F}_{c,l}^{i}\right)^2}}{\frac{1}{N_{col}} \sum_{c=0}^{N_{col}} \left|\hat{F}_{c,l}^{i}\right|},$$

where $N_{qty}$, $N_{lev}$, $N_{col}$ are the number of radiative quantities (e.g., heating rates, surface fluxes, top of atmosphere fluxes) in the cost function, the number of vertical levels for each radiative quantity and the number of atmospheric profiles or columns used for the evaluation. $F$ and $\hat{F}$ are the fluxes or heating rates computed with the $k$-distribution and with the line-by-line radiative transfer model (Clough et al., 2005), respectively.

The root mean square errors of radiative heating rates are computed and normalized for each vertical layer separately. While this approach may break in narrow spectral intervals, where heating rates are zero in some vertical layers, we only consider broadband fluxes and heating rates.

## Data Availability Statement

Data and scripts generated and used for this paper are available on Zenodo (Veerman et al., 2023).

**Acknowledgments**
M.V. and C.v.H. acknowledge funding from the Dutch Research Council (NWO) (Grant: VI.Vidi.192.068). The simulations were carried out on the Dutch national e-infrastructure with the support of SURF Cooperative. R.P. and E.M. acknowledge funding from the U.S. National Oceanic and Atmospheric Administration (NOAA) (Grant; NA21OAR4590161) and the U.S. Department of Energy (DOE) (Grant; SC0021262).

## References

Brown, A. R., Cederwall, R. T., Chlond, A., Duynkerke, P. G., Golaz, J.-C., Khairoutdinov, M., et al. (2002). Large-eddy simulation of the diurnal cycle of shallow cumulus convection over land. *Quarterly Journal of the Royal Meteorological Society*, *128*(582), 1075–1093. https://doi.org/10.1256/003590002320373210

Chung, E.-S., & Soden, B. J. (2015). An assessment of direct radiative forcing, radiative adjustments, and radiative feedbacks in coupled ocean–atmosphere models. *Journal of Climate*, *28*(10), 4152–4170. https://doi.org/10.1175/JCLI-D-14-00436.1

Clough, S., Shephard, M., Mlawer, E., Delamere, J., Iacono, M., Cady-Pereira, K., et al. (2005). Atmospheric radiative transfer modeling: A summary of the AER codes. *Journal of Quantitative Spectroscopy and Radiative Transfer*, *91*(2), 233–244. https://doi.org/10.1016/j.jqsrt.2004.05.058

Duynkerke, P. G., de Roode, S. R., van Zanten, M. C., Calvo, J., Cuxart, J., Cheinet, S., et al. (2004). Observations and numerical simulations of the diurnal cycle of the EUROCS stratocumulus case. *Quarterly Journal of the Royal Meteorological Society: A Journal of the Atmospheric Sciences, Applied Meteorology and Physical Oceanography*, *130*(604), 3269–3296. https://doi.org/10.1256/qj.03.139

Fu, Q., & Liou, K. N. (1992). On the correlated $k$-distribution method for radiative transfer in nonhomogeneous atmospheres. *Journal of the Atmospheric Sciences*, *49*(22), 2139–2156. https://doi.org/10.1175/1520-0469(1992)049⟨2139:OTCDMF⟩2.0.CO;2

Garand, L., Turner, D. S., Larocque, M., Bates, J., Boukabara, S., Brunel, P., et al. (2001). Radiance and Jacobian intercomparison of radiative transfer models applied to HIRS and AMSU channels. *Journal of Geophysical Research*, *106*(D20), 24017–24031. https://doi.org/10.1029/2000JD000184

Gristey, J. J., Feingold, G., Glenn, I. B., Schmidt, K. S., & Chen, H. (2020). Surface solar irradiance in continental shallow cumulus fields: Observations and large-eddy simulation. *Journal of the Atmospheric Sciences*, *77*(3), 1065–1080. https://doi.org/10.1175/JAS-D-19-0261.1

Gustafson, W. I., Vogelmann, A. M., Li, Z., Cheng, X., Dumas, K. K., Endo, S., et al. (2020). The large-eddy simulation (LES) atmospheric radiation measurement (ARM) symbiotic simulation and observation (LASSO) activity for continental shallow convection. *Bulletin of the American Meteorological Society*, *101*(4), E462–E479. https://doi.org/10.1175/BAMS-D-19-0065.1

Hersbach, H., Bell, B., Berrisford, P., Hirahara, S., Horányi, A., Muñoz-Sabater, J., et al. (2020). The ERA5 global reanalysis. *Quarterly Journal of the Royal Meteorological Society*, *146*(730), 1999–2049. https://doi.org/10.1002/qj.3803

Hogan, R. J., & Matricardi, M. (2022). A tool for generating fast $k$-distribution gas-optics models for weather and climate applications. *Journal of Advances in Modeling Earth Systems*, *14*(10), e2022MS003033. https://doi.org/10.1029/2022MS003033

Iacono, M. J., Delamere, J. S., Mlawer, E. J., Shephard, M. W., Clough, S. A., & Collins, W. D. (2008). Radiative forcing by long-lived greenhouse gases: Calculations with the AER radiative transfer models. *Journal of Geophysical Research*, *113*(D13), D13103. https://doi.org/10.1029/2008JD009944

Iacono, M. J., Mlawer, E. J., Clough, S. A., & Morcrette, J.-J. (2000). Impact of an improved longwave radiation model, RRTM, on the energy budget and thermodynamic properties of the NCAR community climate model, CCM3. *Journal of Geophysical Research*, *105*(D11), 14873–14890. https://doi.org/10.1029/2000JD900091

Klinger, C., Mayer, B., Jakub, F., Zinner, T., Park, S.-B., & Gentine, P. (2017). Effects of 3-d thermal radiation on the development of a shallow cumulus cloud field. *Atmospheric Chemistry and Physics*, *17*(8), 5477–5500. https://doi.org/10.5194/acp-17-5477-2017

Mlawer, E. J., Taubman, S. J., Brown, P. D., Iacono, M. J., & Clough, S. A. (1997). Radiative transfer for inhomogeneous atmospheres: RRTM, a validated correlated-$k$ model for the longwave. *Journal of Geophysical Research*, *102*(D14), 16663–16682. https://doi.org/10.1029/97JD00237

Pincus, R., Forster, P. M., & Stevens, B. (2016). The radiative forcing model intercomparison project (RFMIP): Experimental protocol for CMIP6. *Geoscientific Model Development*, *9*(9), 3447–3460. https://doi.org/10.5194/gmd-9-3447-2016

Pincus, R., Mlawer, E. J., & Delamere, J. S. (2019). Balancing accuracy, efficiency, and flexibility in radiation calculations for dynamical models. *Journal of Advances in Modeling Earth Systems*, *11*(10), 3074–3089. https://doi.org/10.1029/2019MS001621

Pincus, R., & Stevens, B. (2009). Monte Carlo spectral integration: A consistent approximation for radiative transfer in large eddy simulations. *Journal of Advances in Modeling Earth Systems*, *1*(2), 1. https://doi.org/10.3894/JAMES.2009.1.1

Rauber, R. M., Stevens, B., Ochs, H. T., Knight, C., Albrecht, B. A., Blyth, A. M., et al. (2007). Rain in shallow cumulus over the ocean: The RICO campaign. *Bulletin of the American Meteorological Society*, *88*(12), 1912–1928. https://doi.org/10.1175/BAMS-88-12-1912

Rothman, L., Jacquemart, D., Barbe, A., Chris Benner, D., Birk, M., Brown, L., et al. (2005). The HITRAN 2004 molecular spectroscopic database. *Journal of Quantitative Spectroscopy and Radiative Transfer*, *96*(2), 139–204. https://doi.org/10.1016/j.jqsrt.2004.10.008

Seifert, A., & Beheng, K. (2006). A two-moment cloud microphysics parameterization for mixed-phase clouds. Part 1: Model description. *Meteorology and Atmospheric Physics*, *92*(1–2), 45–66. https://doi.org/10.1007/s00703-005-0112-4

Seifert, A., Heus, T., Pincus, R., & Stevens, B. (2015). Large-eddy simulation of the transient and near-equilibrium behavior of precipitating shallow convection. *Journal of Advances in Modeling Earth Systems*, *7*(4), 1918–1937. https://doi.org/10.1002/2015MS000489

Sekiguchi, M., & Nakajima, T. (2008). A $k$-distribution-based radiation code and its computational optimization for an atmospheric general circulation model. *Journal of Quantitative Spectroscopy and Radiative Transfer*, *109*(17), 2779–2793. https://doi.org/10.1016/j.jqsrt.2008.07.013

Siebesma, A. P., Bretherton, C. S., Brown, A., Chlond, A., Cuxart, J., Duynkerke, P. G., et al. (2003). A large eddy simulation intercomparison study of shallow cumulus convection. *Journal of the Atmospheric Sciences*, *60*(10), 1201–1219. https://doi.org/10.1175/1520-0469(2003)60⟨1201:ALESIS⟩2.0.CO;2

Stevens, B., & Seifert, A. (2008). Understanding macrophysical outcomes of microphysical choices in simulations of shallow cumulus convection. *Journal of the Meteorological Society of Japan*, *86A*, 143–162. https://doi.org/10.2151/jmsj.86A.143

Tijhuis, M., van Stratum, B., & van Heerwaarden, C. C. (2022). An efficient parameterization for surface 3d radiative effects in large-eddy simulations. *Earth and Space Science Open Archive*, *17*. https://doi.org/10.1002/essoar.10511758.1

Tomita, H. (2008). New microphysical schemes with five and six categories by diagnostic generation of cloud ice. *Journal of the Meteorological Society of Japan*, *86A*, 121–142. https://doi.org/10.2151/jmsj.86A.121

van Heerwaarden, C. C., van Stratum, B. J. H., Heus, T., Gibbs, J. A., Fedorovich, E., & Mellado, J. P. (2017). MicroHH 1.0: A computational fluid dynamics code for direct numerical simulation and large-eddy simulation of atmospheric boundary layer flows. *Geoscientific Model Development*, *10*(8), 3145–3165. https://doi.org/10.5194/gmd-10-3145-2017

van Zanten, M. C., Stevens, B., Nuijens, L., Siebesma, A. P., Ackerman, A. S., Burnet, F., et al. (2011). Controls on precipitation and cloudiness in simulations of trade-wind cumulus as observed during RICO. *Journal of Advances in Modeling Earth Systems*, *3*(2), M06001. https://doi.org/10.1029/2011MS000056

Veerman, M. A., Pincus, R., Mlawer, E. J., & van Heerwaarden, C. C. (2023). Cloud-resolving simulations with radiative transfer at reduced spectral resolution [Dataset]. Zenodo. https://doi.org/10.5281/zenodo.8138305

Wing, A. A., Reed, K. A., Satoh, M., Stevens, B., Bony, S., & Ohno, T. (2018). Radiative–convective equilibrium model intercomparison project. *Geoscientific Model Development*, *11*(2), 793–813. https://doi.org/10.5194/gmd-11-793-2018

Wing, A. A., Stauffer, C. L., Becker, T., Reed, K. A., Ahn, M.-S., Arnold, N. P., et al. (2020). Clouds and convective self-aggregation in a multimodel ensemble of radiative-convective equilibrium simulations. *Journal of Advances in Modeling Earth Systems*, *12*(9), e2020MS002138. https://doi.org/10.1029/2020MS002138

Zhang, M., & Huang, Y. (2014). Radiative forcing of quadrupling $CO_2$. *Journal of Climate*, *27*(7), 2496–2508. https://doi.org/10.1175/JCLI-D-13-00535.1